



Bottom boundary layer spectral dissipation estimates in the presence of wave motions

T. F. GROSS,* A. J. WILLIAMS† and E. A. TERRAY†

(Received 27 January 1993; in revised form 15 December 1993; accepted 22 December 1993)

Abstract—Turbulence measurements are an essential element of the Sediment TRansport Events on Shelves and Slopes experiment (STRESS). Sediment transport under waves is initiated within the wave boundary layer at the seabed, at most a few tens of centimeters deep. The suspended load is carried by turbulent diffusion above the wave boundary layer. Quantification of the turbulent diffusion active above the wave boundary layer requires estimates of shear stress or energy dissipation in the presence of oscillating flows. Measurements by Benthic Acoustic Stress Sensors of velocity fluctuations were used to derive the dissipation rate from the energy level of the spectral inertial range (the $-5/3$ spectrum). When the wave orbital velocity is of similar magnitude to the mean flow, kinematic effects on the estimation techniques of stress and dissipation must be included. Throughout the STRESS experiment there was always significant wave energy affecting the turbulent bottom boundary layer. LUMLEY and TERRAY [(1983) *Journal of Physical Oceanography*, 13, 2000–2007] presented a theory describing the effect of orbital motions on kinetic energy spectra. Their model is used here with observations of spectra taken within a turbulent boundary layer which is affected by wave motion. While their method was an explicit solution for circular wave orbits aligned with mean current we extrapolated it to the case of near bed horizontal motions, not aligned with the current. The necessity of accounting for wave orbital motion is demonstrated, but variability within the field setting limited our certainty of the improvement in accuracy the corrections afforded.

1. INTRODUCTION

TURBULENCE in the bottom boundary layer is described by a number of parameters. The shear velocity scale which characterizes the bed shear stress is probably the most important. Measurements of it depend upon velocity profiles or direct turbulent velocity component correlations. These techniques have been used extensively and have well known difficulties (GRANT and MADSEN, 1986; GROSS *et al.*, 1992). The indirect measure of shear stress through the turbulent kinetic energy dissipation has recently been receiving attention (GROSS and NOWELL, 1986; HUNTLEY, 1988; GREEN, 1992; AGRAWAL *et al.*, 1992). This method uses a high resolution current meter to provide an estimate of the velocity power spectrum. The spectral amplitude of the inertial energy range is a function of the energy dissipation. This technique apparently overcomes the principal difficulty of the profile method technique by requiring a measurement at only one level above the seabed.

*Skidaway Institute of Oceanography, Savannah, GA 31416, U.S.A.

†Woods Hole Oceanographic Institute, Woods Hole, MA 02543, U.S.A.

The requirements for applicability of the spectral dissipation technique appear rather stringent. The turbulent boundary layer must have a sufficiently large Reynolds number to assure the existence of an inertial subrange (TENNEKES and LUMLEY, 1972). The measurement must be taken within the logarithmic layer but at a distance from the bed where mean flow shear is small relative to dissipation scale shear. The height of measurement must be great enough that the local Reynolds number is large, $u_* z \kappa / \nu > Re_c \approx 3000-4000$, but low enough to be within the constant stress region of the logarithmic layer, $z < 0.05-0.10 \kappa u_* / f$ (where u_* is turbulent shear velocity scale, z is height above bottom, κ is von Karman's constant, ν is viscosity, and f is Coriolis frequency). HUNTLEY (1988) demonstrates that these requirements are met only for u_* greater than 0.8 cm s^{-1} . Luckily, sediment transport of silts, sands and cohesive muds require u_* in excess of 1.0 cm s^{-1} and the spectral technique may yet be of use for transport studies.

An additional requirement of the spectral technique is the absence of interfering length or time scales. The presence of up-stream separated flow, such as about a large boulder, will interfere with the local balance of energy production and energy dissipation and prevent the development of the inertial cascade region. However simple motions such as the oscillation due to surface gravity waves may be dealt with. Gravity wave motion transports the smallest dissipative eddies past the measurement point effectively aliasing wave motion into higher frequencies. It is important to realize that this is a kinematic effect and does not necessarily imply a dynamic effect upon the energy cascade. LUMLEY and TERRAY (1983) develop the method of extracting the shape and amplitude of the inertial $-5/3$ slope spectra from Eulerian measures of the velocity time series and frequency spectra. The present study uses this technique to apply the spectral dissipation method to a data set which contains a variety of wave conditions.

The STRESS experiment sought to collect a data set to interpret the turbulent boundary layer and sediment transport under conditions of strong forcing by swell and local wind wave events. A variety of instruments were deployed, including the Benthic Acoustic Stress Sensor (BASS) current meter system used to measure turbulent vector velocities through the logarithmic region of the bottom boundary layer. The BASS data can be applied to the spectral energy dissipation estimation technique at up to six levels above the bed. A comparison of spectral estimates of u_* to more classical u_* estimation techniques such as logarithmic profile fitting can be made. Half-hourly data were taken for several months providing a variety of flow conditions.

The spectral dissipation estimation method appears to work well in controlled environments with simple mean currents. The STRESS experiment included a good deal of strong wave forcing. Corrections for wave advection effects on inertial range spectra have been put forward. These techniques of widening the spectral dissipation technique to wave boundary layer flows should be tested in an environment where the control cases can be identified with periods of simple mean flow only. However at the STRESS site it was found that even though wave energy spanned two decades, there was always wave motion large enough to affect the spectra.

2. DISSIPATION FROM ENERGY SPECTRA

LUMLEY and TERRAY (1983) present a development of the effect of wave and drift motions upon the turbulence spectra. Using their nomenclature, the turbulence is described by the spectral tensor:

$$\Phi_{ij}(\vec{k}) = \frac{E(k)}{4\pi k^2} [\delta_{ij} - k_i k_j / k^2] \quad (1)$$

where k_i is a component of the wave number vector, δ_{ij} is the Kronecker delta and the scalar energy density in the inertial subrange of isotropic, well developed turbulence, is assumed to be:

$$E(k) = \alpha \varepsilon^{2/3} k^{-5/3} \quad (2)$$

where ε is the kinetic energy dissipation. The integral of the spectral tensor over all wave numbers and directions is defined to be the total variance, $u_i u_i$, or twice the kinetic energy. The integral of the scalar isotropic energy density over the modulus of \vec{k} is defined to be the kinetic energy.

$$KE = \frac{1}{2} (u'^2 + v'^2 + w'^2) = \frac{1}{2} \iiint_{-\infty}^{+\infty} \Phi_{ii}(\vec{k}) dk_x dk_y dk_z = \int_0^{\infty} E(k) dk. \quad (3)$$

These definitions ultimately affect the value of the constant a in equation (2). The one-dimensional spectra for variance parallel to the integration direction, $\overline{u'^2} = \int_0^{\infty} F_{11}(k_1) dk_1$, and variance perpendicular to the integration direction, $\overline{v'^2} = \overline{w'^2} = \int_0^{\infty} F_{22}(k_1) dk_1$, have the same functional form as $E(k)$ within the inertial range.

$$F_{11}(k_1) = \alpha \varepsilon^{2/3} k_1^{-5/3} \quad (4)$$

$$F_{22}(k_1) = 3/4 \alpha \varepsilon^{2/3} k_1^{-5/3} \quad (5)$$

where α has been found from lab and field experiments ($\alpha = 0.5$, WYNGAARD and COTE, 1971). The 3/4 factor accounts for the scaling difference between longitudinal and transverse spectra. This value for α corresponds to $a = 1.5$ (TENNEKES and LUMLEY, 1972).

The $-5/3$ slope form of the inertial subrange spectra is theoretically known for wave number k . If the energy density spectrum can be measured then the dissipation rate, ε , can be obtained. However most techniques measure the energy density spectrum at a fixed point as a function of frequency, not of wave number. The time series can be related to a wave number description through Taylor's hypothesis of frozen turbulence, where the time scale of rotation of an eddy of wave number, k , is long compared to the time scale of motion of the eddy past the measurement point. The dynamic time scale of a turbulent eddy from the inertial range is $t_t = \varepsilon^{-1/3} k^{-2/3} = l^{1/3} k^{-2/3} u^{-1}$ where the rate of dissipation $\varepsilon \approx u^3/l$ scales with turbulent velocity scale, u , and shear scale, l . The drift time scale of the eddy, advected by mean velocity U_d , is $t_d = (kU_d)^{-1}$. The frozen turbulence hypothesis will apply directly if,

$$t_t \gg t_d \quad (6)$$

$$(kl)^{1/3} \gg u/U_d. \quad (7)$$

When this criterion is met the dissipation may be extracted from the frequency spectra of the velocity time series:

$$S_{ij}(\omega) = \int_{-\infty}^{+\infty} \exp(-i\omega t) \rho_{ij}(t) dt / 2\pi \quad (8)$$

where $\rho_{ij} = \overline{u_i(0)u_j(t)}$ is the velocity correlation function. The dissipation is obtained from the $-5/3$ slope in the inertial frequency range of the spectra:

$$\varepsilon = [S_{11}\omega^{5/3}U_d^{-2/3}\alpha^{-1}]^{3/2}. \quad (9)$$

This method has been successfully applied to marine boundary layers only a few times (BOWDEN, 1962; GRANT *et al.*, 1984; GROSS and NOWELL, 1985; HUNTLEY, 1988; GREEN, 1992). The required condition of equation (6) is difficult to achieve in practice. However, even more difficult to obtain is a natural flow which is devoid of time scales other than t_i and t_d . Often surface gravity waves interfere by introducing an oscillation time scale which is intermediate to t_i and t_d .

LUMLEY and TERRAY (1983) introduced the methodology for handling the effect on inertial energy density of mean drift and wave advection. In the limit of frequencies ω , large compared to the wave frequency, ω_o , and when the wave motion may be neglected compared to drift motion, the horizontal streamwise spectrum is,

$$S_{11}(\omega) \rightarrow \frac{9}{55} a\varepsilon^{2/3}U_d^{2/3}\omega^{-5/3}. \quad (10)$$

The pure advection result with $2(9/55)a = \alpha$. When drift effects are negligible compared with wave advection, the spectrum is given by

$$S_{11}(\omega) \rightarrow \frac{7}{110} 2^{1/3}\Gamma\left(\frac{1}{3}\right)a\varepsilon^{2/3}(\omega_o R)^{2/3}\omega^{-5/3} \quad (11)$$

where R is the at depth orbital radius of the gravity wave, ($\omega_o R$ is the orbital velocity of the wave). We have directly replaced $\omega_o \eta_{rms}$ in Lumley and Terray's equation (4.7) with $\omega_o R$, because R is here defined to be the full wave excursion length scale at depth, already incorporating the probability distribution of Lumley and Terray's equation (4.7) for the Rayleigh spread of a narrow wave height spectrum. This is in accord with their use of R in equation (4.11) [our equation (13)].

The intermediate case, when wave orbital velocity is of similar magnitude to the drift velocity ($\omega_o R/U_d \approx 1$), is a more complicated function which describes combined effects from both wave advection and drift advection. The derivation of LUMLEY and TERRAY'S (1983) solution is outlined here to point out the relevant non-dimensional numbers which control the solution. The intermediate solution first requires a harmonic decomposition of the frequency spectrum:

$$S_{11}(\omega) = \sum_{n=-\infty}^{+\infty} S_n(\omega). \quad (12)$$

Within the inertial range a simplified form of S_n is obtained:

$$S_n(\omega) = \frac{a\varepsilon^{2/3}R^{5/3}}{5\sqrt{\pi}U_d} \frac{\Gamma(1/3)}{\Gamma(5/6)} K_n(\beta_n) \quad (13)$$

where

$$K_n(\beta_n) = \int_{\beta_n}^{+\infty} \frac{\exp[-x^2]I_n(x^2)}{x^{5/3}(x^2 - \beta_n^2)^{1/2}} [1 - 8\beta_n^2/11x^2] dx \quad (14)$$

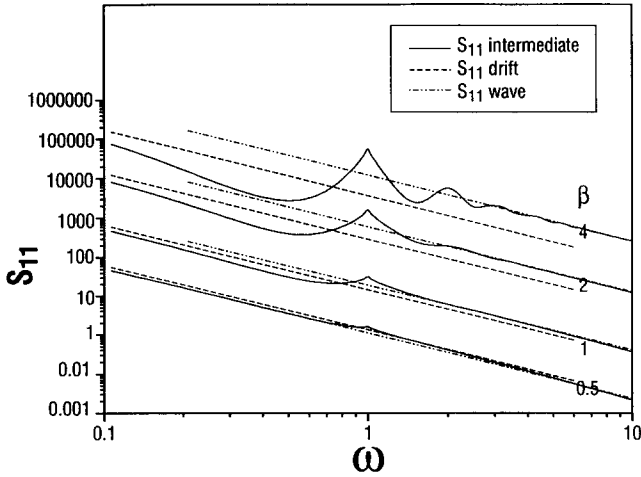


Fig. 1. The series solution for S_{11} , equations (12)–(15), is compared to the advection dominated, equation (10), and wave dominated, equation (11), solutions of S_{11} for different values of $\beta = \omega_o R/U_d$.

with

$$\beta_n = \beta \left| \frac{\omega}{\omega_o} - n \right|. \tag{15}$$

LUMLEY and TERRAY’s (1983) intermediate solution, equations (12)–(15), is evaluated numerically. The form of the solution is a strong function of $\beta = \omega_o R/U_d$. The STRESS data set includes estimates of U_d , ω_o and R as well as half-hourly estimates of the energy spectra $S_{22}(\omega)$. Therefore the parameter β is given and equations (12)–(15) can be evaluated for ε . Because the wave field is seldom monotonic, the solution is not exact. However it can be used to refine estimates of dissipation.

As β ranges in value from 0.01 to 10.0 the intermediate solution moves from the pure advection situation $\beta < 0.1$ to wave dominated $\beta > 2.0$ (Fig. 1). For small β , relatively large advective velocity, the intermediate solution is well approximated by the advection formulation, equation (10). For large beta, $\beta \geq 1.0$, relatively large wave motion, the intermediate solution is best modeled by equation (11). Evaluation of the accurate numerical solution to the intermediate case is computationally difficult (several iterative solutions are required involving two-dimensional integrals). Rather than solve this for each experimentally determined β , a graph of the ratio of the intermediate solution to the two asymptotic solutions evaluated at a frequency of six times the wave frequency was prepared (Fig. 2). The coefficient, C_β , is obtained from these curves by using the ratio $C_\beta = S_I/S_{low}$ when $\beta < 0.2$ and using $C_\beta = S_I/S_{high}$ when $\beta > 0.2$. The coefficient will be used with the observed spectra, S_{22} , to estimate dissipation, ε , with the correction for wave motions:

$$\varepsilon = \left[\frac{C_\beta S_{22}(6\omega_o)}{\frac{9}{55} a U_d^{2/3} (6\omega_o)^{-5/3}} \right]^{3/2} \quad \beta < 0.2 \tag{16}$$

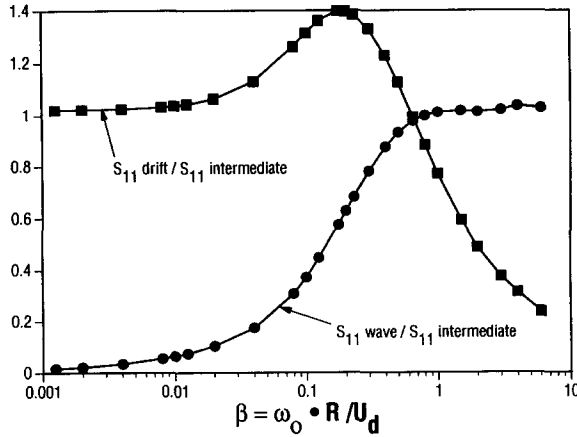


Fig. 2. The ratio between the intermediate solution and the asymptotic solutions, C_β , is plotted vs β . The ratio is evaluated at frequency $\omega = 6\omega_o$. Solid line is ratio to wave dominated high ω asymptote. Dashed line is ratio to advection dominated low ω asymptote.

$$\varepsilon = \left[\frac{C_\beta S_{22}(6\omega_o)}{\frac{7}{6} \frac{9}{55} a(\omega_o R)^{2/3} (6\omega_o)^{-5/3}} \right]^{3/2} \quad \beta > 0.2. \tag{17}$$

The coefficient is evaluated at $6\omega_o$ because this is relatively high compared to ω_o , for $\beta < 4$, and within the resolution range of our data set. The Nyquist frequency of our spectra is $2\pi \times 1 \text{ s}^{-1}$, so the spectra are clearly resolved at $\approx 2\pi \times 0.5 \text{ s}^{-1}$. The average wave periods are longer than 12 s and wave energy is usually at a frequency lower than $\omega_o = 2\pi/12 \text{ s}^{-1}$, which gives $6\omega_o = 2\pi \times 0.5 \text{ s}^{-1}$, within the well resolved range of the measured spectrum.

The LUMLEY and TERRAY (1983) method for near surface wind generated wave motion is not exactly applicable to the present near bed wave motion situation. Their model describes waves moving parallel to the drift direction and near the surface where the wave orbital motion describes a circle. These two assumptions of their model were useful in solving integrals which otherwise would have nested two deeper and not yielded to the expansion solution, equations (12)–(15). The bottom boundary layer wave motions are horizontal and can be at any angle to the current. Orbital shape and orientation to mean current describe the path the measurement point moves over as it scans past the isotropic wave number field describing the energy tensor, equation (1). Inclusion of these effects does not alter the total energy estimates but does alter the perceived distribution between along-stream and cross-stream components. As the ratio between these components is of order 0.75–1.3 the large effect of wave advection can be adequately described by equations (16) and (17).

Estimation of the dissipation based on equations (16) and (17) are calculated from the STRESS data set. The appropriate equation will be chosen based on the value of β . Because the boundary layer velocity shear can be large at any one time the value of β may vary across the profile by a factor of two. If the combined effect of waves and drift were ignored and either equations (10) or (11) were used alone the spectral wavenumber level would be derived from the frequency spectra with errors as indicated by the two crossing curves of Fig. 2. This would not be an important observation unless values of β spanned the

intermediate range where the errors could be the largest. It was observed that, within the STRESS data set, times with β outside this range are rare. The correction for wave motion effects upon the dissipation estimates is a first order consideration.

3. METHODS

The Sediment TRansport Events on Shelves and Slopes (STRESS), experiment was designed to measure the data pertinent to sediment suspension and transport events (NOWELL *et al.*, 1987). On the Northern California coast off Stewarts Point in the vicinity of the CODE experiments the forcing of the bottom boundary layer is a combination of along-shore currents and swell or wind driven waves (BEARDSLEY and LENTZ, 1987; CACCHIONE and DRAKE, 1990). The STRESS site is on the central shelf where the bottom slope is $\approx 5 \times 10^{-3}$. The bottom is uniformly roughened by ripples of a few centimeters in height and animal tracks and trails of millimeter scale etched in the $15 \mu\text{m}$ mean grain sized sediment (CACCHIONE *et al.*, 1983).

The emphasis of the STRESS experiment was the bottom boundary layer. Therefore detailed measurements of turbulence, wave and mean currents were made within 5 m of the bed with the BASS instrument platform (WILLIAMS *et al.*, 1987). The BASS instrument is a 5 m high bottom landing tripod with six small triaxial acoustic velocity sensors arrayed to profile turbulent velocity vectors at up to 5 Hz. This deployment of BASS differed from previous experiments by utilizing a 20 Megabyte data logger. This large storage capacity allowed high data rates to be recorded for extended periods. In addition the data logger's computer was programmed to perform *in situ* Fourier transforms of the 2 Hz data, ensemble average and compress the results for storage. The fundamental recording period was once every half-hour. The full half-hour averages and cross products were recorded for all six BASS current meters. Temperature, and transmissometer data were recorded at 10 min intervals.

Fourier transforms of pressure, horizontal velocity vector at two levels and vertical velocity component at four levels [40 cm a.b. (above bed), 76 cm a.b., 135 cm a.b. and 196 cm a.b.], were calculated *in situ* and recorded every half-hour. The third BASS current meter, at 135 cm a.b., had a persistent noise problem so we plot data from only three levels. The fourth pod, at 196 cm a.b., also had intermittent noise, but not as seriously as pod 3. The 2 Hz turbulence data stream was stored for the first 17.0 min of each half-hour. The 17 min of data were analyzed in four segments of 512 points each with a 24 bit resolution Integer FFT (MONRO, 1977). The resultant 4 min power spectra were ensemble averaged and recorded. The low frequency range ($1/256 \text{ s}^{-1}$ to $1/6.6 \text{ s}^{-1}$) of the horizontal spectra were recorded. The wave motion amplitude and frequency were obtained from the horizontal spectra. The high frequency range from $1/4.7 \text{ s}^{-1}$ to $1/1.3 \text{ s}^{-1}$ were block averaged to 15 estimates of spectral power in frequency bands of $1/25 \text{ s}^{-1}$ width. The one dimensional power spectra were rotated to stream line coordinates and scaled to variance:

$$\begin{aligned} \overline{u'^2} &= \int F_{11}(\omega) d\omega \\ \overline{w'^2} &= \int F_{22}(\omega) d\omega. \end{aligned} \quad (18)$$

The accuracy of the 24 bit IFFT was checked against a full floating point FFT implementation. Once each 21 h (the disk record write cycle) the full 17 min of unaltered 2 Hz data, which was IFFT'd, was recorded. The data was analyzed and compared with the

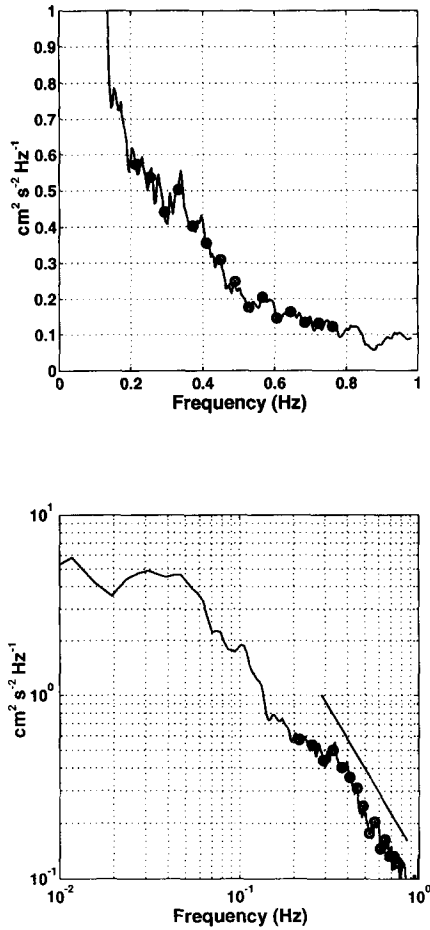


Fig. 3. Frequency spectrum of vertical velocity evaluated with full data set, solid line, and with the *in situ* integer FFT, circles. A line of slope $f^{-5/3}$ is shown in the logarithmic plot.

in situ processed data. The *in situ* IFFT was verified to be in agreement to the level of accuracy recorded; $1 \text{ bit} = 2.166e - 05 \text{ cm}^2 \text{ s}^{-2} \text{ Hz}^{-1}$ (Fig. 3). However, upon occasion there were velocity measurement “dropouts”. These occurred as either discrete spikes or periods of erroneously high variance or noise. The effect on the IFFT was a several order of magnitude jump in the spectral level which is easily identified and eliminated from the processed data.

Uncertainty in estimations of $F_{22}(\omega)$, U_d and $\omega_o R$ result in uncertainties in estimates of ε [equation (16)]. Essentially the single estimate of ε obtained by averaging across frequencies of the spectrum is a spectral estimate with $4 \text{ spectra} \times 15 \text{ frequency band samples} \times 10 \text{ degrees of freedom per band}$ equal to 600 degrees of freedom. The 95% confidence limits of the spectral estimate, $S(\omega)$, are 0.86–1.18, or for $S^{3/2}$, 0.79–1.28. The 95% uncertainty bounds for a 30 min average of velocity were found to be approximately $2.07\sqrt{0.4^2/40} \approx 2.06 \times 0.08 \approx 0.16$ (GROSS *et al.*, 1992). The 15 min 95% confidence interval for \bar{U} is thus $\pm 23\%$. The errors in equation (16) compound to result in ε error

bounds of 0.65–1.66. A reduction of these error bounds may be achieved by averaging adjacent half-hourly estimates resulting in hourly resolution.

The velocity and wave data were analyzed as in GROSS *et al.*, 1992 yielding half-hourly estimates of wave frequency, wave orbital excursion distance and wave orbital velocity. The half hour averaged velocity data were used to obtain estimates of the logarithmic velocity profile parameters from a least squares regression to the lowest five current meters:

$$\bar{U}(z) = \frac{u_*}{\kappa} \ln \frac{z}{z_o} \quad (19)$$

The sixth meter at 493 cm a.b. was often anomalous because it was above the logarithmic layer and was excluded from the regression analysis.

4. RESULTS

The STRESS experiment was designed to identify the variety of flow situations occurring during the winter storm season. The magnitudes of current speeds and wave orbital velocities were quite variable throughout the data set. Speed mainly varies with tides and maximum speeds are found as tidal pulses. Wave intensity is concentrated in a few storm events. The non-storm normal background nearly always has some wave energy. A few sample periods are extracted emphasizing the variety of conditions of wave–current interaction. Figure 4 shows a period of high mean current (10–15 cm s⁻¹) and

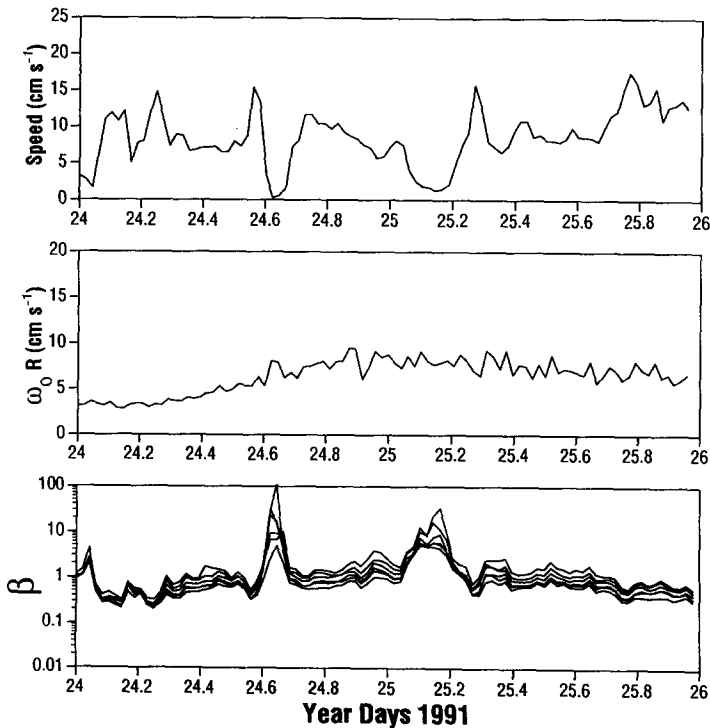


Fig. 4. BASS data for a period of high speed and moderate waves. Year days 24–26. (a) \bar{U} , mean speed at 2 m a.b. (b) $\omega_o R$, wave orbital velocity at 2 m a.b. (c) $\beta = \omega_o R / \bar{U}$.

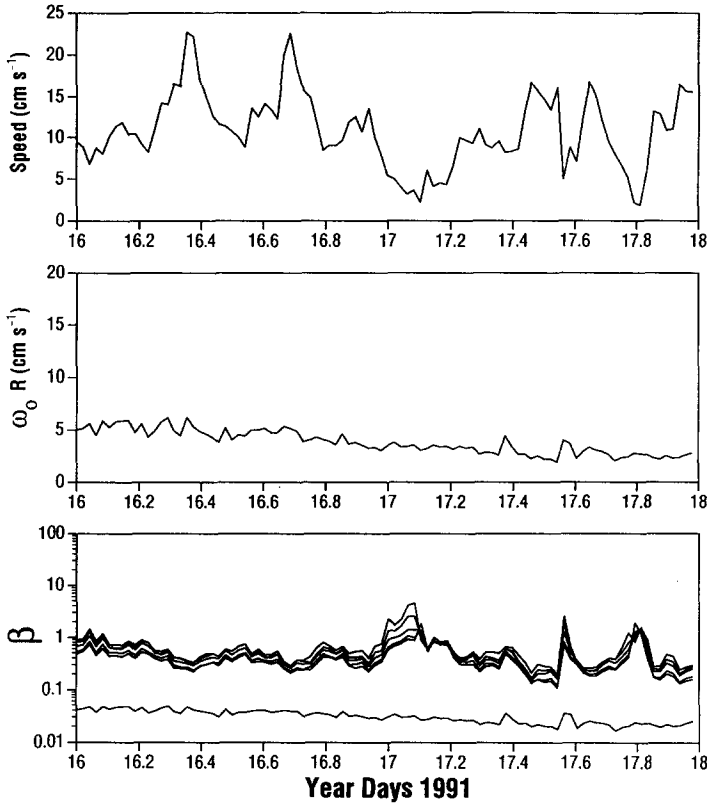


Fig. 5. BASS data for a period of high speed and low waves. Year days 16–18. (a) \bar{U} , mean speed at 2 m a.b. (b) $\omega_o R$, wave orbital velocity at 2 m a.b. (c) $\beta = \omega_o R / \bar{U}$.

moderate wave orbital velocity ($\omega_o R = 8 \text{ cm s}^{-1}$) which occurred on days 24–26. Figure 5 highlights a period of large mean current (up to 23 cm s^{-1}) and low waves ($\omega_o R < 5 \text{ cm s}^{-1}$) which occurred on days 16–18. Figure 6 shows a period of low mean current ($5\text{--}10 \text{ cm s}^{-1}$) and high waves ($\omega_o R > 10 \text{ cm s}^{-1}$) which occurred on days 14–16. Finally, Fig. 7 shows a period of low mean current ($\sim 5 \text{ cm s}^{-1}$) and low waves ($\omega_o R < 2 \text{ cm s}^{-1}$) which occurred on days 27–29.

Following Gross *et al.* (1992) the logarithmic velocity profile was fit by least squares to the data of Figs 4, 5, 6 and 7. Because each time period has different physical forcing processes the error bars for each time period are calculated separately. The Student statistic, $Z = \frac{1}{2} \text{atanh } R$, based on the regression coefficients, R did show some differences between the time segments. The values of Z and R are rather similar between time periods, however the periods of low waves had the lowest R and therefore the greatest errors, Table 1.

In situations when the wave motion is small the physical roughness dominates the log regression intercept, and z_o would remain fairly constant and relatively small $\approx 0.1 \text{ cm}$ (Gross *et al.*, 1992). When waves are present the mean flow boundary layer and the wave boundary layer interact to produce an effective roughness which is much larger than the physical roughness. This effect is well explained by the wave–current interaction model of

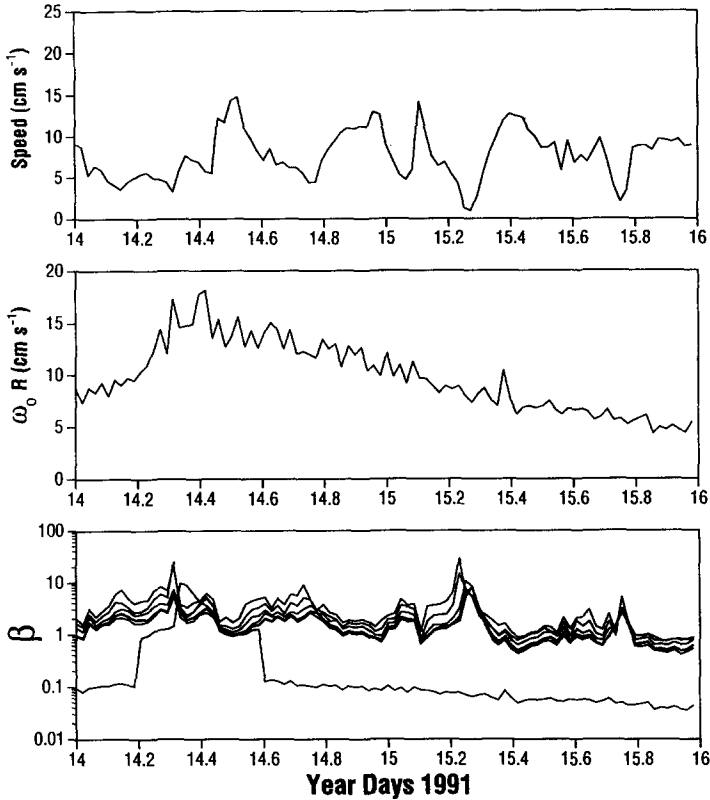


Fig. 6. BASS data for a period of low speed and high waves. Year days 14–16. (a) \bar{U} , mean speed at 2 m a.b. (b) $\omega_o R$, wave orbital velocity at 2 m a.b. (c) $\beta = \omega_o R / \bar{U}$.

GRANT and MADSEN (1979), and was discussed for the STRESS experiment in GROSS *et al.* (1992). If two profiles of similar mean velocity are compared the one with the larger z_o will demonstrate greater shear and spread in velocities at the levels of the current meters. The variance about the mean explained by the slope is a greater percentage of the total variance when the slope is large. The regression coefficient, the variance explained by the slope as a fraction of the total variance, can be larger for larger z_o (all other factors remaining constant). Thus, the period with largest mean velocity and minimal waves has lower R^2 and larger error bands than the two periods with substantial wave action. The presence of waves has the counter-intuitive effect of increasing regression coefficients.

The value of β is plotted for the current meters during each time segment [Figs 4(c), 5(c), 6(c) and 7(c)]. Due to the gradient in $\bar{U}(z)$ near the bed, the spread of β across the profile is as much as 50%. Figure 2 shows that as long as β is either small, $\beta < 0.1$, or large, $\beta > 1.0$, this spread of β would have little effect on the relative values of ϵ . However for the intermediate values a large variation is obtained and plots of $\epsilon(z)$ will be affected. Notice that because \bar{U} ranges from 2 to 25 cm s^{-1} and $\omega_o R$ ranges from 2 to 18 cm s^{-1} the range of β is largely constrained to the range 0.1–10.0. This is the range of the intermediate solution, between the asymptotes of Fig. 2. Most of the data set requires the wave-kinetic interaction in its description.

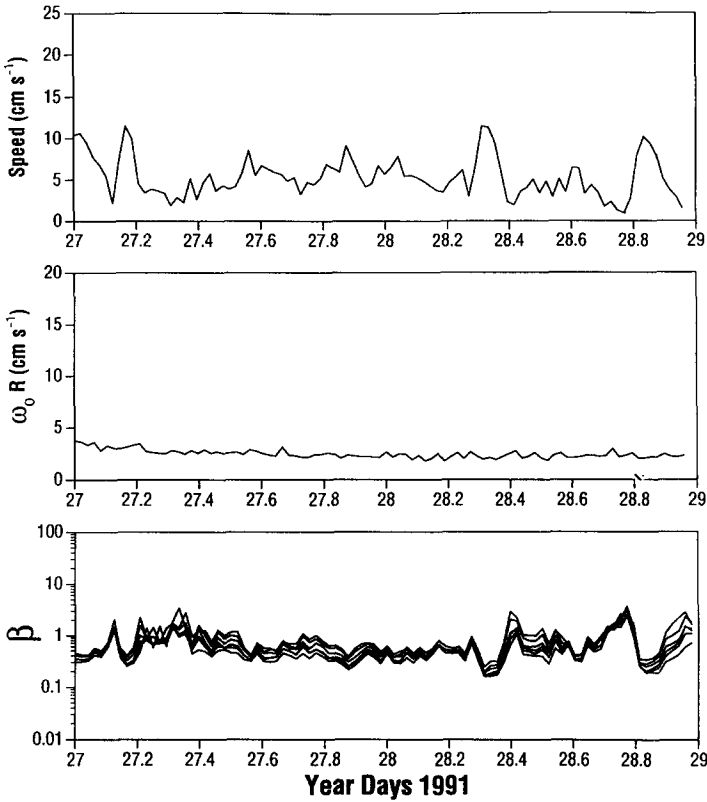


Fig. 7. BASS data for a period of low speed and low waves. Year days 27–29. (a) \bar{U} , mean speed of 2 m a.b. (b) $\omega_0 R$, wave orbital velocity at 2 m a.b. (c) $\beta = \omega_0 R / \bar{U}$.

The dissipation estimates appear noisy but perhaps the time series is not much noisier than expected for the confidence range of $0.65\text{--}1.66 \bar{\epsilon}$. Within these confidence bounds there is no discernible difference between dissipation at heights 40 cm a.b. and 76 cm a.b. This is somewhat surprising as the dissipation within the logarithmic region is expected to be inversely proportional to height. However near constant dissipation near the bed has been noted previously (GROSS and NOWELL, 1986; HUNTLEY, 1988; GREEN, 1992).

Within the logarithmic velocity profile region, steady state balance of shear produced energy with dissipation predicts the simple equation for shear velocity scale, u_* :

Table 1. Ninety-five per cent confidence ranges

		Days	\bar{Z}	R	95% confidence ranges	
					u_*	z_0
High \bar{U}	Mid Wave	24–26	2.61	0.989	$\pm 19\%$	$\times/2.50$
High \bar{U}	Low Wave	16–18	2.29	0.980	$\pm 26\%$	$\times/3.54$
Low \bar{U}	High Wave	14–16	2.40	0.984	$\pm 24\%$	$\times/3.12$
Low \bar{U}	Low Wave	27–29	2.29	0.980	$\pm 25\%$	$\times/3.56$

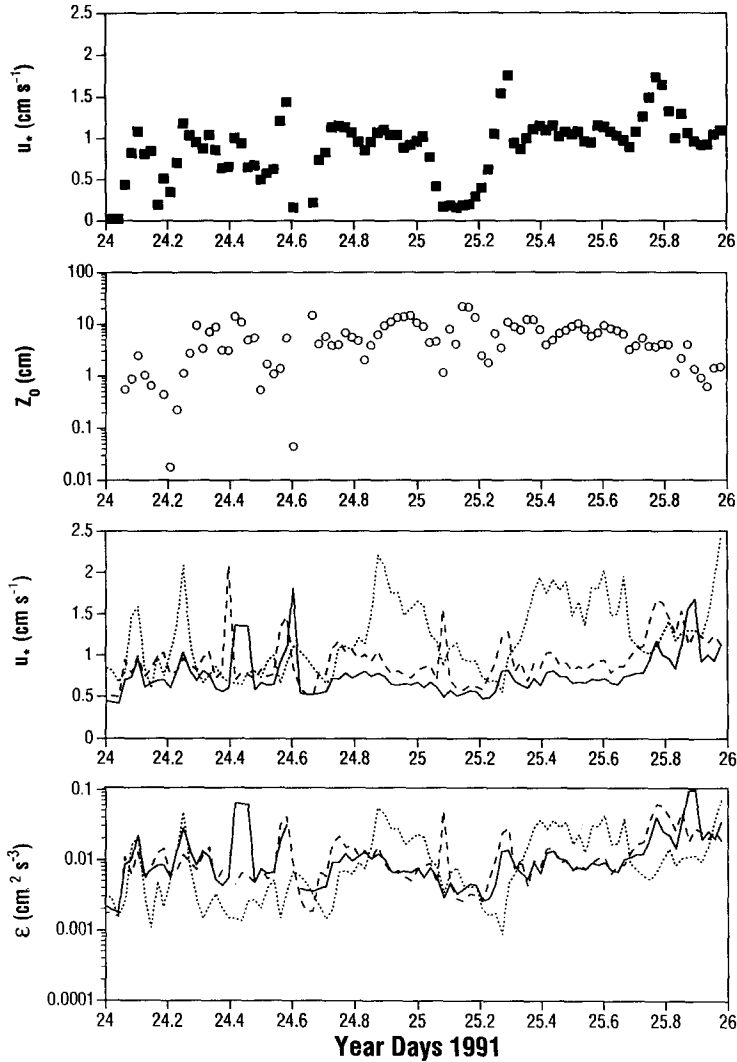


Fig. 8. BASS data for a period of high speed and moderate waves. Year days 24–26. (a) u_* , estimates from least squares fit to velocity profile. (b) z_0 , estimates from least squares fit to velocity profile. (c) $u_* = (\kappa z \epsilon)^{1/3}$ based upon dissipation values obtained from spectra (–40 cm a.b., –76 cm a.b., . . . 196 cm a.b.). (d) ϵ , dissipation estimates derived from amplitude of vertical spectra in inertial subrange (–40 cm a.b., –76 cm a.b., . . . 196 cm a.b.).

$$u_* = (\epsilon \kappa z)^{1/3}. \quad (20)$$

This estimate for u_* has also been plotted in Figs 8–11. The one-third power of ϵ results in a much smoother time series than the dissipation estimates (note the change from logarithmic to linear scales in Figs 8–11). The uniformity in z of the dissipation results in a gradient of u_* estimates, where the estimates from closest to the bed are uniformly less than those from higher up. Nevertheless, the spectral estimate of u_* agrees with the least squares u_* within their combined error bounds. The spectral estimate of u_* appears to have a minimal

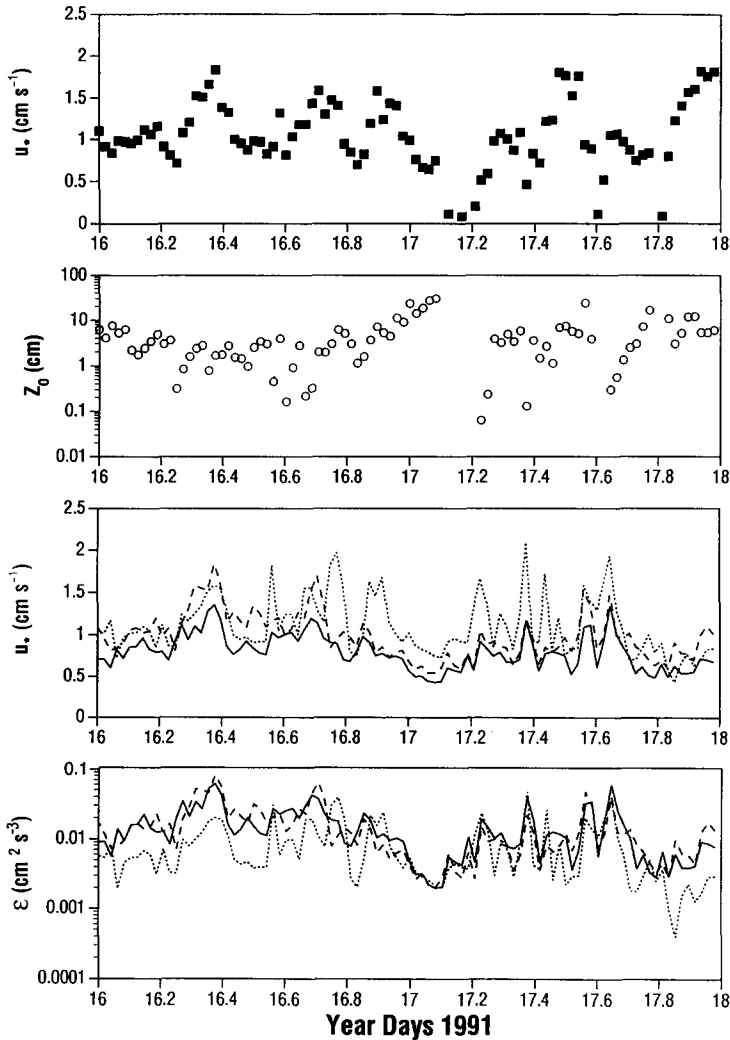


Fig. 9. BASS data for a period of high speed and low waves. Year days 16–18. (a) u_* , estimates from least squares fit to velocity profile. (b) z_0 , estimates from least squares fit to velocity profile. (c) $u_* = (\kappa z \epsilon)^{1/3}$ based upon dissipation values obtained from spectra. (—40 cm a.b., - - -76 cm a.b., . . . 196 cm a.b.). (d) ϵ , dissipation estimates derived from amplitude of vertical spectra in inertial subrange (—40 cm a.b., - - -76 cm a.b., . . . 196 cm a.b.).

value of $\approx 0.5 \text{ cm s}^{-1}$. HUNTLEY (1988) has shown that for u_* below 0.8 cm s^{-1} the assumptions which lead to equation (20) are violated. When u_* is less than 0.5 cm s^{-1} the assumptions of steady state balance between local production and dissipation and a fully developed inertial range, are violated. Dissipation which exceeds local shear production, or an inertial spectral band which is elevated, may be the result of advected or diffused energy. The presence of an energetic wave boundary layer below a slow mean current could provide the source of such advected energy. When β is large (strong waves, weak current), the temporal variability of ϵ appears to decrease and the depth dependence also

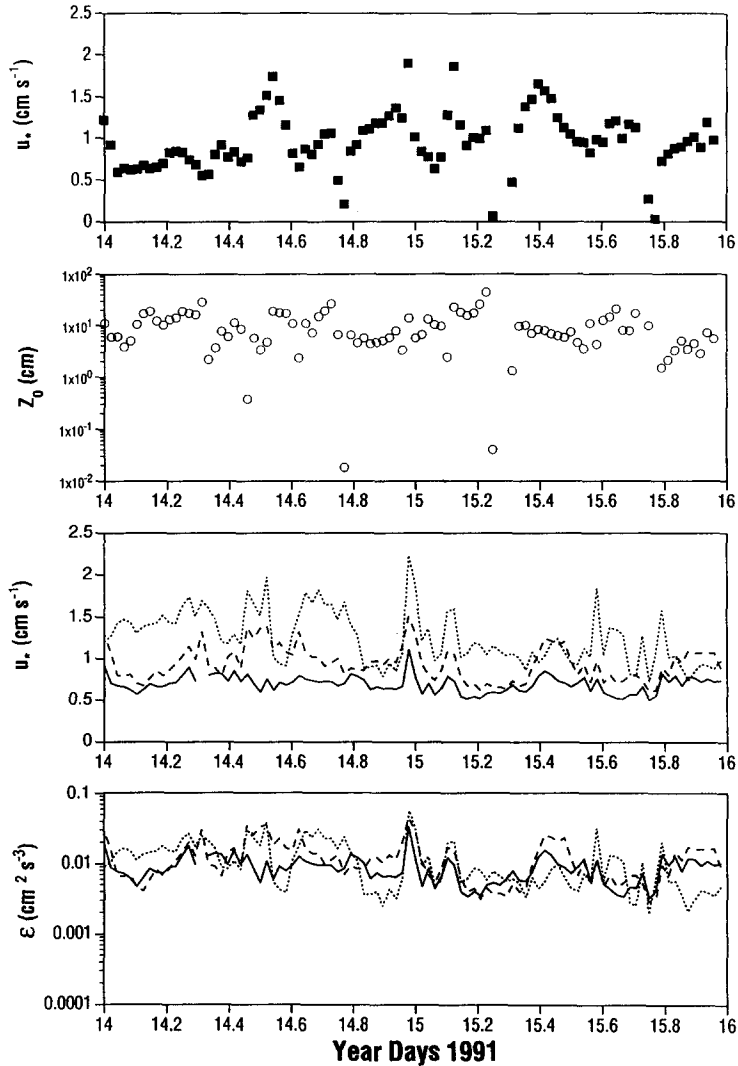


Fig. 10. BASS data for a period of low speed and high waves. Year days 14–16. (a) u_* , estimates from least squares fit to velocity profile. (b) z_0 , estimates from least squares fit to velocity profile. (c) $u_* = (\kappa z \epsilon)^{1/3}$ based upon dissipation values obtained from spectra (–40 cm a.b., –76 cm a.b., . . . 196 cm a.b.). (d) ϵ , dissipation estimates derived from amplitude of vertical spectra in inertial subrange (–40 cm a.b., –76 cm a.b., . . . 196 cm a.b.).

decreases (note times near 24.65, 25.25, 17.0 and 15.2 y.d. in Figs 8–10). This reinforces the idea of an energetic wave boundary layer of energy providing a source of advected energy which would not scale with local height.

5. SUMMARY

The spectra recorded *in situ* by the BASS instrument promised an alternative method to obtain long time series of the shear stress velocity, u_* . The difficulty and expense of

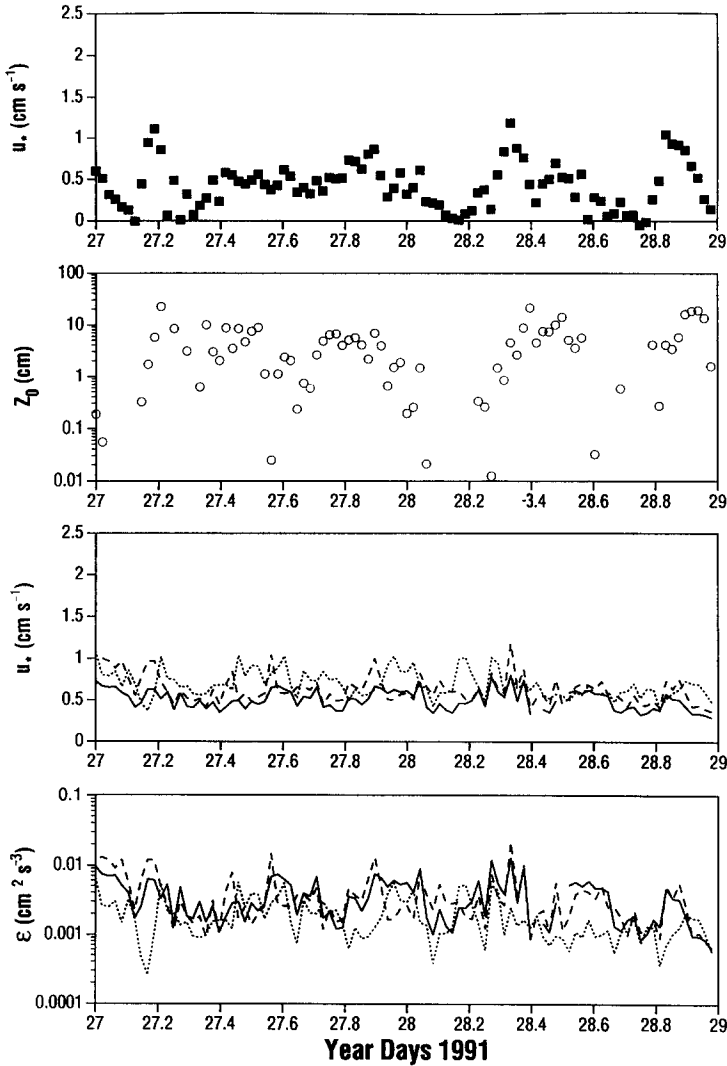


Fig. 11. BASS data for a period of low speed and low waves. Year days 27–29. (a) u_* estimates from least squares fit to velocity profile. (b) z_0 , estimates from least squares fit to velocity profile. (c) $u_* = (kz\varepsilon)^{1/3}$ based upon dissipation values obtained from spectra (–40 cm a.b., –76 cm a.b. . . . 196 cm a.b.). (d) ε , dissipation estimates derived from amplitude of vertical spectra in inertial subrange (–40 cm a.b., –76 cm a.b., . . . 196 cm a.b.).

obtaining four or more mean velocities within the logarithmic velocity layer, from which a profile based estimate of u_* can be obtained, are great. Therefore dissipation based estimates of the turbulence velocity scale from a single current meter time series was thought to provide an economy and perhaps an improvement for boundary layer monitoring methods. The results fell short of the promise.

The wave motions included in the STRESS data sets are sufficient to affect the turbulent bottom boundary layer without dominating it fully (Gross *et al.*, 1992). The $-5/3$ spectral

slope was found to be developed a decade above the wave frequency. Spectral estimates of dissipation were obtained after correction for the kinematic effects of combined wave and drift currents. Non-uniformity in time or space may be responsible for the large scatter in dissipation estimates. Dissipation has a log-normal probability distribution which results in considerable scatter even between 15 min averages (AGRAWAL *et al.*, 1992). The assumptions of sufficiently large spatial separation of shear generating length scales from molecular dissipation length scales are demanding. The mean flow must be large ($15\text{--}25\text{ cm s}^{-1}$) to achieve this scale separation and a logarithmic velocity profile at the STRESS site.

Comparison of the results of the two methods pointed out the short comings of each. First a satisfactory comparison is possible mainly because the optimal expected uncertainties of both estimation techniques is rather large, $\approx \pm 0.25u_*$ for the profile method, and $\approx \pm 0.20u_*$ for the spectral technique. Second, the constraints placed upon the spectral technique by assumptions of sufficient scale allowed comparison only when u_* was greater than $\approx 0.8\text{ cm s}^{-1}$. Finally both methods require conditions for a fully developed logarithmic velocity profile region. The spectral technique has not expanded the realm of measurement opportunities. A profile of u_* estimates may allow some additional averaging. But with an estimate at only one level the method is no substitute for the velocity profile method.

Finally the utility of mean profile stress and energy levels above a wave boundary layer must be questioned. Although mean flow fields certainly advect the suspended sediment the critical shear stress at the bed is clearly dominated by wave stress. The *in situ* spectral measurements of wave amplitude and frequency have proven to be a more useful descriptor of sediment transport potential than the spectral estimates of energy dissipation above the wave boundary layer.

Acknowledgement—This contribution to the STRESS program was made possible by a grant from the Office of Naval Research, N00014-90-J-1046.

REFERENCES

- ABRAMOWITZ M. and I. Q. STEGUN, editors (1964) *Handbook of mathematical functions*, National Bureau of Standards, 1046 pp.
- AGRAWAL Y. C., E. A. TERRAY, M. A. DONELAN, P. A. HWANG, A. J. WILLIAMS III, W. M. DRENNAN, K. K. KAHMA and S. A. KITAIGORODSKII (1992) Enhanced dissipation of kinetic energy beneath surface waves. *Nature*, **359**, 219–220.
- BEARDSLEY R. C. and S. J. LENTZ (1987) The Coastal Ocean Dynamics Experiment Collection: an Introduction. *Journal of Geophysical Research*, **92** (C2), 1455–1464.
- BOWDEN K. F. (1962) Turbulence. In *The sea*, Vol. 1, M. N. HILL, editor, Wiley-Interscience, New York, pp. 802–825.
- CACCHIONE D. A. and D. E. DRAKE (1990) Shelf sediment transport: an overview with applications to the Northern California continental shelf. In *Sea Vol. 9: Ocean engineering science*, John Wiley and Sons, Inc., New York, pp. 729–773.
- GRANT W. E. and O. S. MADSEN (1979) Combined wave and current interaction with a rough bottom. *Journal of Geophysical Research*, **84** (C4), 1797–1808.
- GRANT W. E. and O. S. MADSEN (1986) The continental shelf bottom boundary layer. *Annual Review of Fluid Mechanics*, **18**, 265–305.
- GRANT W. D., A. J. WILLIAMS III and S. M. GLENN (1984) Bottom stress estimates and their prediction on the Northern California Continental shelf during CODE-1: the importance of wave–current interaction. *Journal of Physical Oceanography*, **14**, 506–527.

- GRANT W. D., A. J. WILLIAMS III and T. F. GROSS (1985) A description of the bottom boundary layer at the HEBBLE site: low frequency forcing, bottom stress and temperature structure. *Marine Geology*, **66**, 219–241.
- GREEN M. O. (1992) Spectral estimates of bed stress at subcritical Reynolds numbers in a tidal boundary layer. *Journal of Physical Oceanography*, **22**, 903–917.
- GROSS T. F. and A. R. M. NOWELL (1985) Spectral scaling in a tidal boundary layer. *Journal of Physical Oceanography*, **15** (5), 496–508.
- GROSS T. F., A. E. ISLEY and C. R. SHERWOOD (1992) Effective roughness changes during storms on the Northern California shelf. *Continental Shelf Research*, **12**, (2/3), 389–414.
- HUNTLEY D. A. (1988) A modified inertial dissipation method for estimating seabed stresses at low Reynolds numbers, with application to wave–current boundary-layer measurements. *Journal of Physical Oceanography*, **18**, 339–346.
- KAIMAL J. C., J. C. WYNGAARD, Y. IZUMI and O. C. COTE (1972) Spectral characteristics of surface layer turbulence. *Quarterly Journal of the Royal Meteorological Society*, **99**, 563–589.
- LUMLEY J. L. and E. A. TERRAY (1983) Kinematics of turbulence convected by a random wave field. *Journal of Physical Oceanography*, **13**, 2000–2007.
- MONRO D. M. (1977) A portable integer FFT in FORTRAN. *Computer Programs in Biomedicine*, **7**, 267–272.
- NOWELL A. R. M., P. A. JUMARS and J. H. KRAVITZ (1987) Sediment Transport Events on Shelves and Slopes (STRESS) and Biological Effects of Coastal Ocean Sediment Transport (BECOST). *EOS*, **68** (35), pp. 722–724.
- TENNEKES H. and J. L. LUMLEY (1972) *A first course in turbulence*, MIT Press, 300 pp.
- WILLIAMS A. J. and T. F. GROSS (1991) *In situ* processing of boundary layer flow measurements for data compression. *IEEE Oceans Proceedings*, **2**, 973–976.
- WILLIAMS A. J., III, J. S. TOCHKO, R. L. KOEHLER, T. F. GROSS, W. D. GRAND and C. V. R. DUNN (1987) Measurement of turbulence with an acoustic current meter array in the oceanic bottom boundary layer. *Journal of Atmospheric and Oceanic Technology*, **4** (2), 312–327.
- WYNGAARD J. C. and O. R. COTE (1972) The budgets of turbulent kinetic energy and temperature variance in the atmospheric surface layer. *Journal of Atmospheric Science*, **28**, 190–201.